Learning-Based Calibration Decision System for Bio-Inertial Motion Application

[1]Sina Askari, [2] Chi-Shih Jao, [2] Yusheng Wang, [1,2]Andrei M. Shkel
[1]Department of Biomedical Engineering, [2]Department of Mechanical and Aerospace Engineering
MicroSystems Laboratory, University of California, Irvine, CA, USA
Email: {*askaris*, *chishihj*, *yushengw*, *andrei.shkel*} @uci.edu

***Abstract*—We developed a learning-based calibration algorithm for a vestibular prosthesis with the long-term goal of reproducing error-free vestibular system dynamic responses. Our approach uses an additional IMU to detect the head acceleration of a patient and to correct the corresponding drift in the vestibular prosthesis. The algorithm includes four major parts. First, we extract features from the shoe-mounted IMU to classify human activities through convolutional neural networks. Second, we fuse data from the head-mounted IMU (vestibular prosthesis). Third, we artificially create additional data samples from a small pool of training data for each classification class. Fourth, we use the classified activities to calibrate the reading from the head-mounted IMU. The results indicate that during daily routine activities the firing rate baseline of a vestibular prosthesis system without calibration fluctuates between $100\,\text{pulses/s}$ to $150\,\text{pulses/s}$; in contrast, an appropriate calibration to human activity results in correction of $4\,\text{pulses/s}$ in extreme cases, providing a stable baseline firing rate while the head is not moving. In this work, we specifically study the contribution of gyroscope scale factor on the drift of the vestibular prosthesis system and propose a corresponding calibration method.**

***Index Terms*—Vestibular prosthesis, multi-sensor fusion, learning algorithm.**

I. Introduction

Proprioception of the body and control of eye movement are supported by the vestibular system of both inner ears. Impairment of one or both sides of vestibular systems, were reported to be caused by, for example, aging, toxic reaction to medications, tumors, or brain injury, resulting in loss of balance, vertigo, abnormal gait, and visual instability [1, 2]. Rotational movements are captured by three semicircular canals and the vector of acceleration (or gravity) is sensed by the otolith organs. Together, the semicircular canals and otolith organs, provide the three-dimensional rotation and translation information of human body to the brain. This information is integrated by the brain with other sensory information and is used for a number of functions, including the posture control and balance, stabilization of images on the retina, and more. For people who have lost vestibular functions, with the help of MEMS inertial sensing technology, position and orientation can be substituted by gyroscopes and accelerometers, which are low in price and small in size, making them suitable for biomedical applications [3]. Vestibular prosthesis uses MEMS Inertial Measurement Unit (IMU) and the corresponding signal processing, which transmits human head rotation to neuronal firing pulses. While MEMS-based Vestibular Prosthesis (VP) has theoretically a potential to restore the balance function, the effect of drift in the sensor on the performance of the vestibular prosthesis may present a major roadblock for acceptance of the technology.

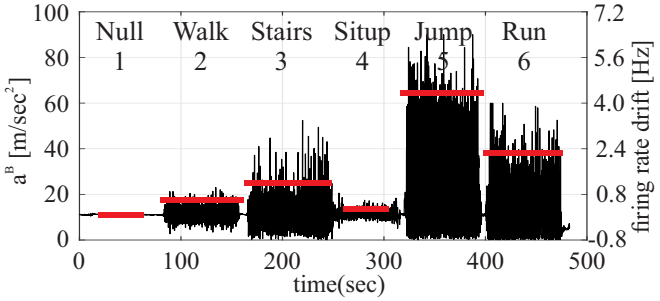

Fig. 1. Acceleration magnitude sensed on head-mounted IMU due to different human activities. Horizontal bar line represents the firing rate drift due to the effect of acceleration, as predicted by the vestibular dynamic model.

We have demonstrated a VP prototype using a single axis commercial grade gyroscope to mimic the dynamics of a vestibular system, [4]. Johns Hopkins University developed a semi-implantable unit with 3 MEMS gyroscopes to restore the vestibular function, [5], and its clinical study is underway to evaluate the unit [6]. Generally, an IMU consists of three orthogonal pairs of gyroscopes and accelerometers to capture the orientation of the sensor with respect to an inertial coordinate frame. For a gyroscope, the scale factor corresponds to sensor's sensitivity, the ratio from a readable output to the input physical rate of rotation, measured in $(\text{Volt or LeastSignificantBit})/(^\circ/\text{s})$. The scale factor of a MEMS gyroscope itself is also sensitive to many factors, such as temperature [7], repeatability (turn-on to turn-on) [8], linearity [9], and acceleration force [10]. For a long duration of operation, inertial sensors require an in-situ multi-dimensional calibration functionality to avoid erroneous signals to be sent to the brain.

The study in [5] proposed a nonlinear dynamic model defining the relationship between head's angular velocity Ω in $[^\circ/\text{s}]$, and the neuron's firing rate in $[\text{pulses/s or Hz}]$ as follows:

$$f = \frac{1}{2} \times f_{max} \times (1 + tanh(tanh^{-1}(2 \times \frac{f_0}{f_{max}} - 1) + C(\frac{\Omega}{450}))),$$

where f_0 is a baseline firing rate at $100\,\text{Hz}$, f_{max} at $450\,\text{Hz}$, C is compression factor of 10 and Ω is input head velocity in $[^\circ/\text{s}]$ with a range between -450 to $450\,^\circ/\text{s}$. According to the model, a typical scale factor sensitivity of $0.1\,^\circ/\text{s/g}$, significantly alters the intensity of the firing rate and could cause an additional vestibular damage or ill-signaling of the vestibular activities. Over daily routine activities, the human body undergoes different accelerations [11], this also applies to the head-mounted IMU, or VP sensor. Fig. 1 demonstrates

978-1-7281-1634-1/19/$31.00 ©2019 IEEE

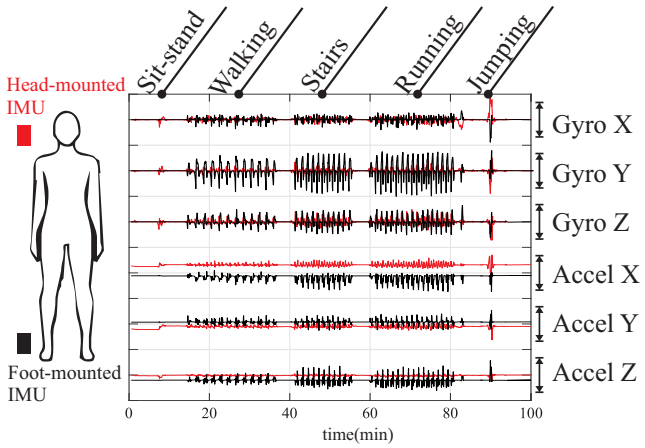

Fig. 2. Demonstration of human daily routine activities recorded by two IMUs, located on foot and head. Each IMU provides 6 parameters.

the corresponding accelerations through the daily routine activities. For the IMU, the sum of magnitudes squared of the acceleration along three axes *(x,y,z)* in the sensor's body coordinate *B* can be represented as:

$$a^B = \sqrt{(a_x^B)^2 + (a_y^B)^2 + (a_z^B)^2},$$

where a^B refers to the magnitude of acceleration experienced by the IMU during each activity. The gyroscope's g-sensitivity is about $0.3\,^\circ/\mathrm{s/g}$ [12], which for VP translates in a drift of $4\,\mathrm{Hz}$ as a result of applied $6.1\,\mathrm{g}$ acceleration, e.g., in the event of jumping, shown also on the plot.

II. Method

A. Data collection

MEMS IMU sensors are categorized into different grades depending on their sensitivity, representing consumer, industrial, tactical, navigation, and space-grades. The consumer grade is easily accessible, smaller in size, low in cost, and often used for biomedical motion applications. The inherent bias and scale factor drifts of such sensors result in a faulty output and corrections become necessary. A major contributing factor to these drifts is environmental changes, such as shock, vibration, and temperature.

In our experiments, data was recorded using three different hardware platforms: a custom foot-mounted inertial navigation system (INS) [13], a miniature GPS-Aided INS, VN-200 [14], and a flexible laboratory INS testbed [15]. The IMUs for each platform were selected to represent different sensor grades, based on their sensitivity and noise characteristics reported by the corresponding manufacturer, including consumer, industrial, and tactical grades, respectively. The head-mounted IMU was mounted behind the ear using straps. Depending on the platform, we attached the foot-mounted IMU either to a custom shoe or strapped on the shoe. Human daily activities were recorded from three different subjects on different days and occasions. An example of motion captured by two IMUs with their location is shown in Fig. 2. Motion signals captured from the two IMUs were different from each other, e.g., more fluctuation in the gyroscope readout was sensed by the foot due to dynamics of the gait and the acceleration pattern across classes (events) was easily distinguishable.

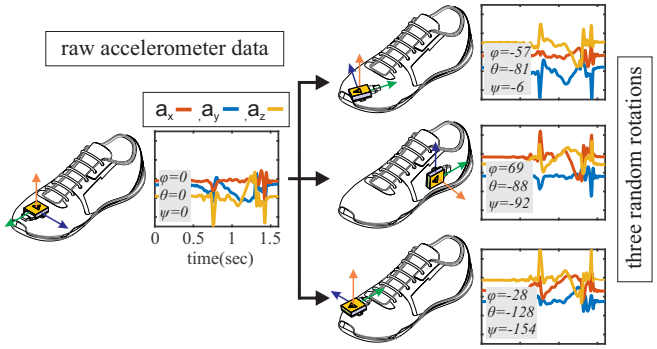

Fig. 3. Data augmentation by 3D rotation of the raw data. Original data (left) compared to rotation angles of ϕ, θ and ψ (right). Only *(x,y,z)* accelerometers from the shoe-mounted IMU are shown for one gait cycle.

B. Data augmentation

The mounting position and the sensor grade of IMU resulted in different accuracy, [16, 17], and the dataset collected for this study was a combination of both approaches. Therefore, the training dataset was rich enough in features. Consequently, to artificially increase the number of training datasets we proposed a data augmentation process inspired by a study in [18]. For every gyroscope and accelerometer recording data in the sensor body-frame coordinates *(x,y,z)*, we applied the Euler rotation, with the corresponding angles ϕ, θ and ψ about the sensor axes using the following sequence of rotations:

$$R_x(\phi,\theta,\psi) = (R_x(\phi)\cdot R_y(\theta)\cdot R_z(\psi)) = \left(\begin{bmatrix}1 & 0 & 0\\ 0 & c(\phi) & s(\phi)\\ 0 & -s(\phi) & c(\phi)\end{bmatrix}\cdot\begin{bmatrix}c(\theta) & 0 & -s(\theta)\\ 0 & 1 & 0\\ s(\theta) & 0 & c(\theta)\end{bmatrix}\cdot\begin{bmatrix}c(\psi) & s(\psi) & 0\\ -s(\psi) & c(\psi) & 0\\ 0 & 0 & 1\end{bmatrix}\right),$$

where *c* and *s* represent *cos* and *sin* functions, respectively. For each dataset, the angles were randomly selected and repeated three times. Fig. 3 illustrates this process visually of the data for one gait cycle.

C. Convolutional Neural Network

Deep learning or multiple-layer neural networks has been successfully applied for image, video, speech, and audio processing [19, 20]. Convolutional Neural Network (CNN) is the first layer in an artificial neural network. CNNs for human event classification using accelerometer alone was demonstrated by [21], and using smartphone IMU by [22]. This study, focuses particularly on shoe-mounted IMU for classification, with expanding the model by fusing the data from a head-mounted IMU. The architecture used for our algorithms is a standard 2D CNNs layer with Rectified linear Unit (RelU) activation followed by a max-pooling layer to train the model [23]. Compared to an image classification, where R, G, B layers are stacked to form a 3D volume with 3 layers depth. In this architecture, the *x, y, z* of gyroscope and accelerometer parameters of both IMUs form a 2D matrix with 1 layer depth, 12 rows and N samples are presented as a column. The width of the matrix represents a sequence in time series extracted from a moving window size of $1.5\,\mathrm{s}$ with an overlap of $0.1\,\mathrm{s}$, which is corresponded to 300 samples at any step. The convolutional layer convolves a matrix weights

window (w) of unit size of $(i \times j)$ on the input temporal sequence (v_i) of IMU data to its neighborhood time window with 64 filters and finally added a bias (b). The RelU layer maps the features from the previous neuron with the following activation function:

$$RelU(v[i] * w[i,j] + b)\ ,\ RelU(x) = \begin{cases} 0 & if \quad x < 0 \\ x & if \quad x >= 0 \end{cases}$$

Followed by the activation function, a 2D global average maximum pooling with stride 2x2 and dropout probability of 20 % were employed to perceive features from the signal [24]. A reshaping layer followed by a dense layer was implemented to fully connect all the previous nodes with 6 output classes for the activity recognition. The datasets were divided into training and testing ratio of 70 % to 30 %.

III. Results

In order to have a sense of features extracted by classification, some basic statistics was computed and correlated with the result from CNNs. Two parameters were extracted from gyroscope and accelerometer datasets: the standard deviation and maximum range (instantaneous difference values across 3-axes during the full gait cycle). These parameters were reported for different activities, as summarized in Table I. The results show that as the speed of the gait cycle increases, e.g., jumping activity, the sensed acceleration and angular motion during the gait cycle increased, which was associated with the signal edges identified by the CNNs.

TABLE I
Features extracted from foot-mounted IMU for classification

	gyroscope (deg/sec)		accelerometer-g (m/s^2)	
Activity/Parameters	max range	std	max range	std
Walking	329.64	185.3	5.48	10.44
Running	567.7	293.89	7.5	14.67
Jumping	938.96	527.02	11.16	22.32
Sit to stand	10.3	3.5	0.5	0.2
Stairs(up & down)	841.3	437.7	6.9	12.90

Four different configurations were considered for classification using the described CNNs: 1) only head-mounted IMU, 2) only foot-mounted IMU, 3) both head- and foot-mounted IMUs, and 4) the same as 3, but with added data augmentation. The visualization of performance of the classification (confusion matrix) is shown in Fig. 4. The head-mounted IMU alone revealed difficulty of distinguishing between walking and running activities, as well as sitting and running activities. The shoe-mounted IMU alone revealed difficulty of distinguishing between standing still from sitting activities, and vice versa. The usage of both IMUs together showed an improvement with the help of data augmentation. The learning rate also increased when utilizing two IMUs, as compared to an individual IMU. The implemented architecture was trained and tested on Google TensorFlow platform. The developed model was applied to the dataset shown earlier in Fig. 1 and the correction was made on the z-axis gyroscope of the head-mounted IMU. The firing rate proportional to the angular velocity before and after correction is shown in Fig. 5. The major benefit of the calibration is to correctly generate

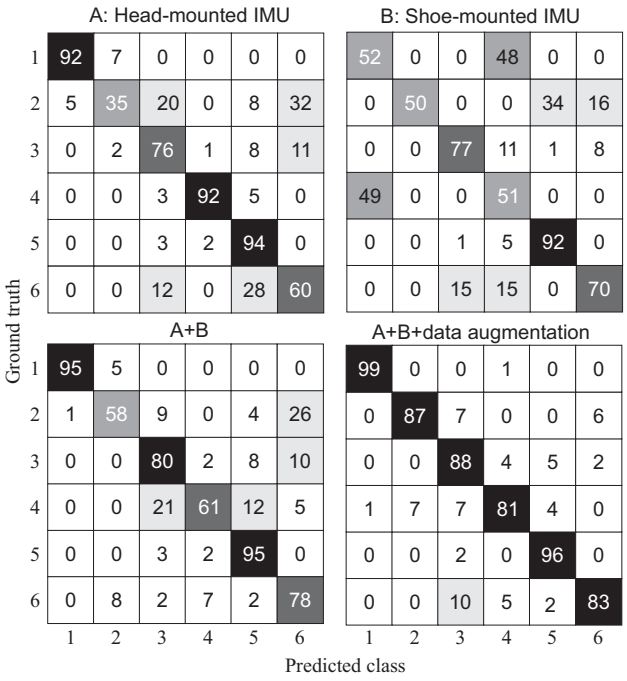

Fig. 4. Confusion matrix on the data set considering four different configurations. Classes are 1)standing still, 2)walking, 3)walking up and down stairs, 4)standing up and sitting down, 5)jumping, and 6)running. Due to rounding of percentages, the summation of each row might not add up to 100.

firing rate for such activities, e.g., in the running activity the largest acceleration force occurs and the necessary corrections are introduced.

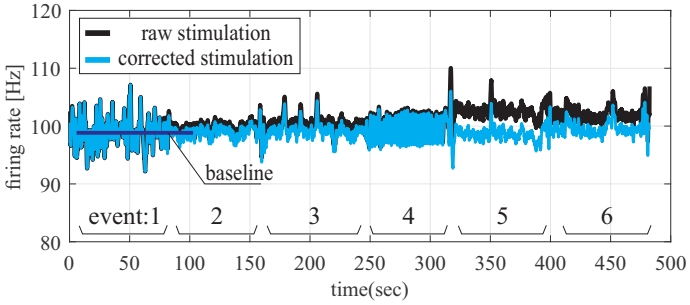

Fig. 5. An example showing a correction of sensitivity of head-mounted IMU using activities, labeled 1 through 6 classifications, to calibrate the z-axis (perpendicular to the transverse plane of the body) proportional to the firing rate.

IV. Conclusion

In this paper we discuss the need for calibration of IMU sensors for accurate reading of motion in the vestibular prosthesis. We proposed a calibration algorithm for the sensor under varying dynamics and environmental conditions. We used convolutional neural networks to classify human activity based on inertial sensor data captured from foot- and head-mounted IMUs. The classification based on a single sensor is shown to be effective, however, fusing multiple sensors resulted in an improved classification. We proposed a data augmentation algorithm for inertial sensors to extend the small dataset and to consider different scenarios of an IMU placement.

ACKNOWLEDGMENT

This work was performed under the following financial assistance award: 70NANB17H192 from U.S. Department of Commerce, National Institute of Standards and Technology (NIST). The author would like to thank Daniel Voronel and Jad Samir Ghosn for their assistant in data collection. The datasets used in this study are available from the corresponding author on request.

REFERENCES

[1] S. J. Herdman and R. Clendaniel, "Bilateral vestibular hypofunction," *Vestibular Disorder Association*, vol. 503, pp. 1–8, 2014.

[2] G. Paige, "Senescence of human visual-vestibular interactions. I. Vestibulo-ocular reflex and adaptive plasticity with aging," *J. Vestibul. Res. Equil.*, vol. 2, no. 2, pp. 133–151, 1992.

[3] C. M. N. Brigante, N. Abbate, A. Basile, A. C. Faulisi, and S. Sessa, "Towards miniaturization of a MEMS-based wearable motion capture system," *IEEE Trans. Ind. Electron.*, vol. 58, no. 8, pp. 3234–3241, 2011.

[4] A. M. Shkel and F.-G. Zeng, "An electronic prosthesis mimicking the dynamic vestibular function," *Audiology and Neurotology*, vol. 11, pp. 113–122, 2006.

[5] C. C. Della Santina, A. A. Migliaccio, and A. H. Patel, "A multichannel semicircular canal neural prosthesis using electrical stimulation to restore 3-D vestibular sensation," *IEEE Trans. Biomed. Eng.*, vol. 54, no. 6 Pt 1, pp. 1016–1030, June 2007.

[6] J. P. Carey, "Multichannel vestibular implant early feasibility study," 2016, https://clinicaltrials.gov/, identifier: NCT02725463.

[7] S. Sonmezoglu, S. E. Alper, and T. Akin, "A high performance automatic mode-matched MEMS gyroscope with an improved thermal stability of the scale factor," in *Int. Conf. Solid-State Sensors and Actuators (TRANSDUCERS)*, Barcelona, Spain, June 16–20, 2013.

[8] J. G. Hanse, "Honeywell MEMS inertial technology & product status," in *IEEE/ION Position Location and Navigation Symposium*, Monterey, CA, USA, Apr 26–29, 2004.

[9] A. Brown and Y. Lu, "Performance test results of an integrated GPS/MEMS inertial navigation package," in *Proceedings of the 17th International Technical Meeting of the Satellite Division of The Institute of Navigation (ION GNSS)*, Long Beach, CA, USA, Sept 21–24, 2004.

[10] B. S. Park, K. Han, S. Lee, and M. Yu, "Analysis of compensation for a g-sensitivity scale-factor error for a MEMS vibratory gyroscope," *J. Micromechanics and Microengineering*, vol. 25, no. 11/115006, pp. 1–10, 2015.

[11] N. Ravi, N. Dandekar, P. Mysore, and M. L. Littman, "Activity recognition from accelerometer data," in *Innovative Applications of Artificial Intelligence (IAAI)*, Pittsburgh, PA, USA, July 9-13, 2005.

[12] J. M. Hansen, J. Rohác, M. Šipoš, T. A. Johansen, and T. I. Fossen, *Validation and Experimental Testing of Observers for Robust GNSS-Aided Inertial Navigation*. Recent Advances in Robotic Systems, InTech, 2016, ISBN (print): 978-953-51-2570-9.

[13] J. Nilsson, A. K. Gupta, and P. Händel, "Foot-mounted inertial navigation made easy," in *IEEE Int. Conf. Indoor Positioning and Indoor Navigation*, Busan, South Korea, Oct 27–30, 2014.

[14] *VN-200 Development Board User Manual*, Vectornav Technologies, Dallas, TX 75238 USA, https://www.vectornav.com/products/vn-200/documentation/.

[15] S. Askari, C.-S. Jao, Y. Wang, and A. M. Shkel, "A laboratory testbed for self-contained navigation," in *IEEE Int. Symp. Inertial Sensors and Systems*, Naples, FL, USA, Apr 1–5, 2019.

[16] Y. Wang, S. Askari, and A. M. Shkel, "Study on mounting position of IMU for better accuracy of ZUPT-aided pedestrian inertial navigation," in *IEEE Int. Symp. Inertial Sensors and Systems*, Naples, FL, USA, Apr 1–5, 2019.

[17] Y. Wang, D. Vatanparvar, A. Chernyshoff, and A. M. Shkel, "Analytical closed-form estimation of position error on ZUPT-augmented pedestrian inertial navigation," *IEEE Sensors Letters*, vol. 2, no. 4, pp. 1–4, 2018.

[18] L. S. Yaeger, R. F. Lyon, and B. J. Webb, "Effective training of a neural network character classifier for word recognition," in *Int. Conf. Neural Inform. Process. Syst. (NeurIPS)*, Denver, CO, USA, Dec 3–5, 1996.

[19] H. Shin, H. R. Roth, M. Gao, L. Lu, Z. Xu, I. Nogues, J. Yao, D. Mollura, and R. M. Summers, "Deep convolutional neural networks for computer-aided detection: CNN architectures, dataset characteristics and transfer learning," in *IEEE Trans. Med. Imag.*, vol. 35, no. 5, 2016, pp. 1285–1298.

[20] Y. LeCun, Y. Bengio, and G. Hinton, "Deep learning," *Nature*, vol. 521, no. 7553, pp. 436–444, 2015.

[21] M. Zeng, L. T. Nguyen, B. Yu, O. J. Mengshoel, J. Zhu, P. Wu, and J. Zhang, "Convolutional neural networks for human activity recognition using mobile sensors," in *Mobile Computing, Applications and Services (MobiCASE)*, Austin, TX, USA, Nov 6-7, 2014.

[22] P. Kasnesis, C. Z. Patrikakis, and I. S. Venieris, "Perceptionnet: A deep convolutional neural network for late sensor fusion," in *Intelligent Syst. Conf.*, London, UK, Sept 6–7, 2018.

[23] Y. LeCun and Y. Bengio, "Convolutional networks for images, speech, and time series," in *The Handbook of Brain Theory and Neural Networks*, M. A. Arbib, Ed. MIT Press, 1998, pp. 255–258.

[24] M. Lin, Q. Chen, and S. Yan, "Network in network," in *Int. Conf. Learn. Representations (ICLR)*, Banff, Canada, Apr 14–16, 2014.